

# Self-consistent Ornstein–Zernike approximation for a binary symmetric fluid mixture

Elisabeth Schöll-Paschinger and Gerhard Kahl

Center for Computational Materials Science and Institut für Theoretische Physik TU Wien,  
Wiedner Hauptstraße 8-10, A-1040 Wien, Austria

(Received 16 October 2002; accepted 9 January 2003)

The self-consistent Ornstein–Zernike approximation (SCOZA) is an advanced microscopic liquid state method that is known to give accurate results in the critical region and for the localization of coexistence curves; this has been confirmed in several applications to continuous and discrete one component systems. In this contribution we present the extension of the SCOZA formalism to the case of a binary symmetric fluid mixture characterized by hard-core potentials with adjacent attractive interactions, given by linear combinations of Yukawa tails. We discuss the stability criteria for such a system and present results for the phase behavior: we recover the well-known three archetypes of phase diagrams, characterized by the different manners the second order demixing line ( $\lambda$ -line) intersects the first order liquid–vapor coexistence curve. © 2003 American Institute of Physics. [DOI: 10.1063/1.1557053]

## I. INTRODUCTION

As we proceed from a one component system to a binary mixture of simple fluids we encounter a considerably enriched variety of phase behavior which is induced by the complex interplay of two phase separation processes: the liquid–vapor transition and the demixing transition. The complex manner of how the now up to four phases can coexist is also reflected in a considerably richer critical behavior: four phase points, critical lines and critical end points (CEPs) now replace the triple point and the simple critical point encountered in a one component fluid. The first attempt to bring order into the rich variety of phase diagrams of binary mixtures was done by Konynenburg and Scott;<sup>1</sup> this *qualitative* study is based on a van der Waals model and is still—to the best of our knowledge—the only systematic work in this field. More *quantitative* investigations which also aim at an accurate determination of the phase diagram (and eventually at a comparison with computer simulation data) are, however, at present out of reach: applications of reliable liquid state methods (such as perturbation theories or integral equation approaches<sup>2</sup>) to determine the phase diagram of a *general* binary mixture are in particular in the binary case considerably more involved than the simple van der Waals analysis, and, in addition, we are now faced with a large number of system parameters. Hence, systematic studies in this field are still out of reach.

Therefore a reasonable starting point to investigate the phase behavior of binary mixtures on a *quantitative* level is to simply reduce the number of system parameters. This can be done by considering a so-called binary *symmetric* mixture; here the interactions between like particles are assumed to be equal [ $\Phi_{11}(r) = \Phi_{22}(r)$ ] while the potential between unlike particles,  $\Phi_{12}(r)$ , is fixed by  $\Phi_{12}(r) = \alpha\Phi_{11}(r)$ .  $\alpha$  and the parameters that characterize the  $\Phi_{ij}(r)$  are the only system parameters; this reduction brings a systematic investigation of the phase behavior of the system within reach.

In fact, already this simplified system shows a rich phase behavior: a mean-field study for this mixture has revealed the following.<sup>3</sup> While for  $\alpha > 1$  only a simple liquid–vapor demixing transition is encountered, the situation is more complex and interesting for  $\alpha < 1$ : here the phase behavior is determined by the interplay of a gas-mixed fluid phase transition and a fluid–fluid demixing transition into a 1-rich and a 2-rich phase, the latter being symmetric with respect to  $x = 1/2$ ,  $x$  being the concentration of species 1. The critical phenomena encountered are critical lines, tricritical points, and CEPs. In the above mentioned study<sup>3</sup> the authors identify three types of phase diagrams (denoted by I, II, and III and discussed in detail in Sec. III B) which are characterized by the different manners the line of the second order demixing transition ( $\lambda$  line) intersects the first order liquid–vapor coexistence line. A fourth type that was observed up to now only in computer simulations<sup>4</sup> has not yet been confirmed in theoretical investigations; its existence is questionable.

In an effort to determine the phase behavior of such a system on a quantitative level one has to use at least thermodynamic perturbation theories or integral equation methods;<sup>2</sup> however, they are known to fail and/or to give unreliable results near phase boundaries and near criticality. To provide in particular in these regions of the phase diagram accurate results, advanced liquid state methods are more appropriate: the self-consistent Ornstein–Zernike approximation (SCOZA)<sup>5</sup> or the hierarchical reference theory (HRT)<sup>6</sup> are two of these methods that have been especially designed to cope with such problems. For a more detailed presentation of the two approaches and an overview we refer to Refs. 7 and 8 (SCOZA) and to Refs. 6 and 9 (HRT).

In this contribution we focus on the SCOZA which is based on a mean spherical (MSA) type closure relation to the Ornstein–Zernike (OZ) equation,<sup>10</sup> replacing the prefactor  $\beta = (k_B T)^{-1}$  in the closure for the direct correlation function by a state dependent, yet undetermined function  $K(\rho, T)$ .

This function is fixed by enforcing thermodynamic consistency between the compressibility and the energy route to the thermodynamic properties; in the one component case this requirement leads to a partial differential equation (PDE) of  $u$ , the excess (over ideal gas) internal energy per volume, in  $T$  and  $\rho$ . Applications of the SCOZA presented up to now to continuum and discrete one component systems have shown that this advanced liquid state approach is indeed able to predict the localization of the critical point and of the coexistence branches within high accuracy (for an overview over these results we refer to Ref. 8). So far, the generalization of the SCOZA to the binary case has been restricted to a lattice gas model.<sup>11</sup>

The success of the SCOZA for continuum one component systems has motivated us to proceed to the binary case: this has been realized in the present contribution for the case of a binary symmetric fluid mixture. Although the SCOZA formalism presented here has been developed for this special binary system, it can be extended (by following similar lines) in a straightforward, but rather tedious way to the *general* binary case. As in all SCOZA applications to continuous systems presented up to now we restrict ourselves to interatomic potentials that consist of a hard-core (HC) part plus an adjacent interaction given by Yukawa tails (HCY interactions). This restriction can be traced back to the fact that the rather heavy formalism of the SCOZA (and its complex numerical implementation) benefits to a considerable amount from the availability of the (semi-)analytic solution of the MSA for a multi-Yukawa, multicomponent HC mixture;<sup>12</sup> a fully numerical solution of the SCOZA, as it would be required for a general potential is at present out of reach.

In the binary case the consistency requirement between the compressibility and the energy route leads to a set of three coupled PDEs of  $u$  in  $T$ ,  $\rho$ , and  $x$ , from which we determine the now three unknown state-dependent functions  $K_{ij}(\rho, T, x)$ . Although in principle a solution algorithm for this formidable problem might be coded, one quickly reaches computational limits. It is now where—in an effort to reduce the complexity of the problem—we have introduced a further simplification in our work: based on symmetry arguments we reduce the  $K_{ij}(\rho, T, x)$  to one single function  $K(\rho, T, x)$ . In addition, by choosing an appropriate linear combination of the three partial consistency relations we are left with only one consistency relation which is now a PDE of  $u$  in  $T$  and  $\rho$ ; as a consequence of the above assumption the PDE can be solved for fixed concentration  $x$ . This assumption is the only approximation in the present work beyond the basic SCOZA assumption that the direct correlation functions outside the cores are proportional to their pair potentials.

Using this extended SCOZA algorithm we have calculated the phase diagram of binary symmetric mixtures, assuming HCY potentials with one single tail: we are thus left with two parameters, the screening length  $z$  and  $\alpha$  (as defined above). Varying for a given  $z$  the parameter  $\alpha$  we obtain, of course, qualitatively the same sequence of phase diagrams as already encountered and labeled in the mean-field study<sup>3</sup> mentioned before. However, both in contrast to a mean-field approach and to conventional liquid state theories we are

now able to approach critical points very closely while still guaranteeing high numerical accuracy. SCOZA thus offers to study critical phenomena of a binary mixture on a *qualitative* level; this will be done in the near future.

For completeness, it should be noted that the HRT (mentioned above) has been applied to binary systems in Refs. 13 and 14. In particular the latter publication is dedicated to a very thorough investigation of the phase diagram of a symmetric binary mixture, discussing—among others—the CEP topology which (in contrast to mean field theories and the SCOZA) is not encountered in the HRT.

The paper is organized as follows: In Sec. II we present the theory, we introduce the system, present the basic ideas of the SCOZA and its formalism for a binary symmetric mixture; the section is closed with numerical remarks and a brief discussion of how to determine limits of stability of a binary mixture within the SCOZA framework. Section III is dedicated to the results: we discuss the limits of stability of the system and present results for the phase diagrams. We close the paper with concluding remarks.

## II. THEORY

### A. The system

In our symmetric binary system with HCY pair potentials  $\Phi_{ij}(r)$  the interaction between the like particles is the same [ $\Phi_{11}(r) = \Phi_{22}(r)$ ], while in the interatomic potentials of unlike particles is given by  $\Phi_{12}(r) = \alpha\Phi_{ii}(r)$ . Thus the repulsive hard-core (HC) is characterized for all three interactions by a diameter  $\sigma$

$$\Phi_{ij}(r) = \begin{cases} \infty, & r \leq \sigma, \\ w_{ij}(r), & r > \sigma. \end{cases} \quad (1)$$

For the  $w_{ij}(r)$ , the attractive tails, we focus on Yukawa potentials, e.g.,

$$w_{11}(r) = -\frac{1}{r} \exp[-z(r-1)]. \quad (2)$$

$z$  is the screening length of the potential; the HC diameter  $\sigma$  and the interaction strength of the attractive tail,  $\epsilon_{11}$ , have been set to unity. Further the mixture is characterized by the total number-density  $\rho$  and the concentration  $x = x_1$  of species 1; partial number densities are defined via  $\rho_1 = x\rho$  and  $\rho_2 = (1-x)\rho$ . We further introduce reduced dimensionless quantities,  $\rho^* = \rho\sigma^3$  and  $T^* = k_B T \sigma / \epsilon_{11}$  where  $T$  is the temperature.

### B. SCOZA—basic ideas

In the case of a *general* binary mixture the SCOZA is based on the OZ relation, which now reads<sup>10</sup>

$$h_{ij}(r) = c_{ij}(r) + \sum_k \rho_k \int d\mathbf{r}' c_{ik}(r') h_{kj}(|\mathbf{r} - \mathbf{r}'|), \quad (3)$$

supplemented by a MSA-type closure relation, i.e.,<sup>5</sup>

$$\begin{aligned} g_{ij}(r) &= 0 \quad \text{for } r \leq 1, \\ c_{ij}(r) &= c_{\text{HC};ij}(r) + K_{ij}(\rho, T, x) w_{ij}(r) \quad \text{for } r > 1. \end{aligned} \quad (4)$$

The  $h_{ij}(r)$  and the  $c_{ij}(r)$  are the total and the direct correlation functions and the  $g_{ij}(r) = h_{ij}(r) + 1$  are the pair distribution functions. The  $c_{\text{HC};ij}(r)$  are the direct correlation functions of the HC reference system.

Different thermodynamic routes establish relations between the thermodynamic and the structural properties of a system. In the binary case, the energy route reads

$$u = 2\pi \sum_{ij} \rho_i \rho_j \int \Phi_{ij}(r) g_{ij}(r) r^2 dr, \quad (5)$$

where  $u$  is the excess (over ideal gas) internal energy per volume; note that  $u = u(\rho, T, x)$ .

The partial compressibility routes establish a link between the chemical potentials  $\mu_i$  and the direct correlation functions via

$$\begin{aligned} \rho_1 \frac{\partial \beta \mu_1}{\partial \rho_1} &= 1 - \rho_1 \tilde{c}_{11}(q=0), \\ \rho_2 \frac{\partial \beta \mu_2}{\partial \rho_2} &= 1 - \rho_2 \tilde{c}_{22}(q=0), \\ \rho_1 \frac{\partial \beta \mu_1}{\partial \rho_2} &= -\rho_1 \tilde{c}_{12}(q=0), \\ \rho_2 \frac{\partial \beta \mu_2}{\partial \rho_1} &= -\rho_2 \tilde{c}_{12}(q=0). \end{aligned} \quad (6)$$

If the  $\mu_i$  and  $u$  stem from a unique Helmholtz free energy, then the partial consistency relations

$$\frac{\partial^2 u}{\partial \rho_i \partial \rho_j} = \frac{\partial}{\partial \beta} \left( \frac{\partial \beta \mu_j}{\partial \rho_i} \right), \quad (7)$$

hold.

In conventional liquid state methods, such as the MSA, different thermodynamic routes lead to different thermodynamic results. In the SCOZA, however, we have the possibility to choose the three yet undetermined functions  $K_{ij}(\rho, T, x)$  in such a way as to guarantee consistency between the energy and the partial compressibility routes. This requirement leads to a coupled set of three PDEs of  $u$  in  $T$ ,  $\rho$ , and  $x$  which fix the unknown functions.

It has turned out, that from the numerical point of view the solution of the PDEs (7) for a general binary mixture is far too complex. The restriction to a binary *symmetric* mixture brings along the following considerable simplifications: first, since all the diameters are equal we can use for  $c_{\text{HC};ij}(r) = c_{\text{HC}}(r)$  the Waisman parametrization for the direct correlation function of the HC reference system<sup>15</sup> (see below); second, the yet undetermined functions  $K_{ij}(\rho, T, x)$  satisfy the following symmetry relations:

$$K_{11}(\rho, T, x) = K_{22}(\rho, T, 1-x), \quad (8)$$

$$K_{12}(\rho, T, x) = K_{12}(\rho, T, 1-x). \quad (9)$$

Under the additional, *simplifying* assumption  $K_{11}(\rho, T, x) = K_{12}(\rho, T, x)$  we end up with one single function  $K(\rho, T, x)$ , that is symmetric with respect to  $x$ ; it is related to the  $K_{ij}$  via

$$K(\rho, T, x) = K_{ij}(\rho, T, x). \quad (10)$$

Instead of the three partial consistency relations (7) we now require only one relation, which we obtain from a suitable linear combination of these relations, like, e.g.,

$$\rho \frac{\partial^2 u}{\partial \rho^2} = \frac{\partial}{\partial \beta} \left( 1 - \frac{1}{\rho} \sum_{ij} \rho_i \rho_j \tilde{c}_{ij}(q=0) \right) = \frac{\partial}{\partial \beta} \left( \frac{1}{\chi_{\text{red}}} \right) \quad (11)$$

with the reduced dimensionless isothermal compressibility  $\chi_{\text{red}} = \rho k_B T \chi_T$  given by

$$\chi_{\text{red}} = \left( \frac{\partial \beta P}{\partial \rho} \right)^{-1}. \quad (12)$$

$\chi_T$  is the isothermal compressibility.

We point out that the left-hand side of (11) is calculated via the energy route while the right-hand side is determined via the compressibility route, enforcing thus consistency between these two thermodynamic routes. As a consequence of the above assumption the concentration  $x$  has become a simple parameter: consequently, the consistency PDE (11) can be solved for different  $x$ -values independently. With the assumption (10) we have added an additional approximation that goes beyond the definition of SCOZA, and we must expect the numerical results to be less highly accurate than those obtained in applications that use nothing but the ansatz that defines SCOZA. To check the accuracy of this additional approximation a detailed comparison with Monte Carlo simulations is planned.<sup>16</sup> Nevertheless, our binary-mixture results capture the full range of critical and tricritical behavior that one would expect in an exact analysis.

### C. SCOZA—formalism

Since the extension of the SCOZA presented here benefits from the availability of the (semi-)analytic solution of the MSA for a HCY system (with an arbitrary number of components and of Yukawa tails), we briefly go back to this solution. Two different approaches to solve the MSA for a HCY system have been proposed in literature: the (original) Laplace transform route<sup>17,18</sup> and the Wiener–Hopf factorization technique introduced by Wertheim<sup>19</sup> and Baxter.<sup>20</sup> The first leads to a rather heavy formalism which forms the basis of the first formulations of the SCOZA. The latter approach is more elegant and more flexible and provides—even for an arbitrary number of components and of Yukawa tails—compact expressions; they are summarized in Ref. 12 in a form suitable for numerical evaluation. Although there has been a great deal of important further development of the application of the Wertheim–Baxter approach to the case of an arbitrary number of Yukawa tails (see Refs. 21–24 and references therein), we know of no formulation in the context of SCOZA or quantitative studies that are directly relevant to use in SCOZA.

Treating the direct correlation function of the HC reference system within the Waisman parametrization with a Yukawa form (details see below), we add another Yukawa tail to the MSA/SCOZA closure relation for the direct correlation function outside the core. Generalization of the SCOZA to the case of an  $m$  component mixture with an arbitrary number of Yukawa tails quickly becomes tedious but should in principle be straightforward.

Under certain conditions,<sup>25</sup> the solution of the OZ equations (3) is equivalent to the solution of the following two integral equations:

$$2\pi r c_{ij}(r) = -Q'_{ij}(r) + \sum_l \rho_l \int_0^\infty Q_{jl}(t) Q'_{il}(r+t) dt, \tag{13}$$

$$2\pi r h_{ij}(r) = -Q'_{ij}(r) + 2\pi \sum_l \rho_l \int_0^\infty (r-t) \times h_{il}(|r-t|) Q_{lj}(t) dt, \tag{14}$$

introducing the so-called factor functions  $Q_{ij}(r)$ .

In the following italic indices are used for the two fluid components while greek indices denote the  $n$  different Yukawa tails. Henceforward, summation over an italic or a greek index corresponds to a summation over the two components of the Yukawa tails, i.e.,

$$\sum_l = \sum_{l=1,2} \quad \text{and} \quad \sum_\nu = \sum_{\nu=1}^n. \tag{15}$$

If the above two integral equations are supplemented by the multi-HCY closure relation

$$h_{ij}(r) = -1, \quad r < 1, \tag{16}$$

$$c_{ij}(r) = \sum_\nu \tilde{K}_{\nu;ij} \frac{e^{-z_\nu(r-1)}}{r}, \quad r > 1,$$

the factor functions must have the following form:

$$Q_{ij}(r) = Q_{ij}^0(r) + \sum_\nu \frac{1}{z_\nu} D_{\nu;ij} e^{-z_\nu(r-1)}, \tag{17}$$

$$Q_{ij}^0(r) = \begin{cases} \frac{a_{ij}}{2}(r-1)^2 + b_{ij}(r-1) \\ + \sum_\nu \frac{1}{z_\nu} C_{\nu;ij} [e^{-z_\nu(r-1)} - 1], & 0 < r < 1, \\ 0, & r > 1. \end{cases} \tag{18}$$

These functions are characterized by 24 yet undetermined coefficients  $a_{ij}$ ,  $b_{ij}$ ,  $C_{\nu;ij}$ , and  $D_{\nu;ij}$ ; in the general case we have  $(2m^2n + 2m^2)$  of these quantities.

Introducing  $G_{\nu;ij}$  via

$$G_{\nu;ij} = z_\nu \int_1^\infty r \exp[-z_\nu(r-1)] g_{ij}(r) dr \tag{19}$$

one can show<sup>12</sup> that the coefficients  $a_{ij}$ ,  $b_{ij}$ ,  $C_{\nu;ij}$  can be expressed in terms of the  $D_{\nu;ij}$  and the  $G_{\nu;ij}$ , which, in turn, satisfy a coupled set of 16 ( $=2m^2n$ ) nonlinear equations,

$$\sum_{\tau,lmk} A_{\tau\nu;mkjl}^{(1)} G_{\tau,km} D_{\tau,m} D_{\nu,il} + \sum_{\tau,lm} A_{\tau\nu;mlj}^{(2)} D_{\tau,m} D_{\nu,il} + \sum_l A_{\nu;jl}^{(3)} D_{\nu,il} + A_{\nu;ij}^{(4)} = 0, \tag{20}$$

$$\sum_{\tau,lmk} B_{\tau\nu;mklj}^{(1)} G_{\tau,km} D_{\tau,mj} G_{\nu,il} + \sum_{\tau,mk} B_{\tau\nu;mkij}^{(2)} G_{\tau,km} D_{\tau,mj}$$

$$+ \sum_{\tau,lm} B_{\tau\nu;mlj}^{(3)} D_{\tau,mj} G_{\nu,il} + \sum_{\tau,m} B_{\tau\nu;mij}^{(4)} D_{\tau,mj} + \sum_l B_{\nu;lj}^{(5)} G_{\nu,il} + B_{\nu;ij}^{(6)} = 0, \tag{21}$$

$$\nu = 1, 2 (=n), \quad i, j = 1, 2 (=m).$$

The explicit expressions for the coefficients  $A$  and  $B$  in the above equations for a general  $m$  component mixture can be found in the Appendix A of Ref. 12.

In particular in the context of the self-consistency problem it should be pointed out that among these quantities the only energy-dependent coefficients are the  $A_{\nu;ij}^{(4)}$ , given as

$$A_{\nu;ij}^{(4)} = 2\pi \tilde{K}_{\nu;ij}, \tag{22}$$

while all the other coefficients are calculated from the  $\rho_i$ , the  $z_\nu$ , and from  $\sigma$ .

The second system of equations (21), is linear in  $\mathbf{D} = \{D_{\nu;ij}\}$  for given  $\mathbf{G} = \{G_{\nu;ij}\}$  and can be written as

$$\sum_{\tau,m} O_{\tau\nu;mij} D_{\tau,mj} = Q_{\nu;ij} \tag{23}$$

with

$$O_{\tau\nu;mij}(\rho, \mathbf{G}) = \sum_{lk} B_{\tau\nu;mkij}^{(1)} G_{\tau,km} G_{\nu,il} + \sum_k B_{\tau\nu;kij}^{(2)} G_{\tau,km} + \sum_l B_{\tau\nu;mlj}^{(3)} G_{\nu,il} + B_{\tau\nu;mij}^{(4)} \tag{24}$$

and

$$Q_{\nu;ij}(\rho, \mathbf{G}) = - \sum_l B_{\nu;lj}^{(5)} G_{\nu,il} - B_{\nu;ij}^{(6)}. \tag{25}$$

Equation (23) has thus the form of a matrix equation

$$\mathbf{O} \cdot \mathbf{D} = \mathbf{Q}. \tag{26}$$

In addition, by suitably arranging the  $D_{\nu;ij}$  in a vector  $\mathbf{D}$  and the  $Q_{\nu;ij}$  in a vector  $\mathbf{Q}$ , one arrives at a block diagonal form for  $\mathbf{O}$ , consisting of 2 ( $=m$ ) blocks of dimension 4 ( $=mn$ ). For the binary symmetric Yukawa fluid with two tails on which we shall focus in this contribution, the vectors  $\mathbf{D}$  and  $\mathbf{Q}$  have the following structure (written as transposed— $T$ —vectors):

$$\mathbf{D}^T = (D_{1;11}, D_{2;11}, D_{1;21}, D_{2;21}, D_{1;12}, D_{2;12}, D_{1;22}, D_{2;22}), \tag{27}$$

$$\mathbf{Q}^T = (Q_{1;11}, Q_{1;21}, Q_{2;11}, Q_{2;21}, Q_{1;12}, Q_{1;22}, Q_{2;12}, Q_{2;22}). \tag{28}$$

Solving the system of 8 ( $=m^2n$ ) linear equations (26) yields  $\mathbf{D}(\rho, \mathbf{G})$ .

In the formulation of the SCOZA we will also need the derivatives  $(\partial \mathbf{D} / \partial \mathbf{G})(\rho, \mathbf{G})$  which are obtained via differentiating Eq. (23),

$$\sum_{\tau,m} O_{\tau\nu; mij}(\rho, \mathbf{G}) \frac{\partial D_{\tau,mj}}{\partial G_{\mu;rs}} = - \left( \sum_{\tau} B_{\mu\nu;srj}^{(1)} G_{\nu;il} + B_{\mu\nu;srij}^{(2)} \right) D_{\mu;sj}(\rho, \mathbf{G}) - \left\{ \sum_{\tau,m} \left( \sum_k B_{\tau\nu;mksj}^{(1)} G_{\tau;km} + B_{\tau\nu;msj}^{(3)} \right) D_{\tau,mj}(\rho, \mathbf{G}) - B_{\nu;s; j}^{(5)} \right\} \delta_{\mu\nu} \delta_{ri}. \quad (29)$$

With all this in mind we now proceed to the SCOZA. Thermodynamic quantities required in the PDE of the SCOZA are the inverse reduced isothermal compressibility and the internal energy, related via the consistency relation (11). The inverse reduced isothermal compressibility calculated via the compressibility route is given by (see Ref. 12)

$$\frac{1}{\chi^{\text{red}}} = \sum_j x_j \left( \frac{A_j}{2\pi} \right)^2, \quad (30)$$

where

$$A_j = A^0(1 + M_j) - 4B^0 N_j \quad (31)$$

with

$$M_j = - \sum_{\tau} \frac{1}{z_{\tau}^2} \sum_m \rho_m \{ M_{\tau}^{(a)} D_{\tau,mj} + (1 - M_{\tau}^{(a)} e^{-z_{\tau}1}) f_{\tau,mj} \},$$

$$N_j = \sum_{\tau} \frac{1}{z_{\tau}^3} \sum_m \rho_m \{ L_{\tau}^{(a)} D_{\tau,mj} + (1 - L_{\tau}^{(a)} e^{-z_{\tau}1}) f_{\tau,mj} \}, \quad (32)$$

$$f_{\tau,mj} = \frac{2\pi}{z_{\tau}^2} \sum_k \rho_k G_{\tau,mk} D_{\tau,kj}.$$

Expressions for  $M_{\tau}^{(a)}$ ,  $L_{\tau}^{(a)}$ ,  $A^0$ , and  $B^0$  in terms of  $\rho_i, z_{\nu}$ , and  $\sigma = 1$  are again compiled in the Appendix A of Ref. 12. Note that indices that have become redundant in these expressions as a consequence of the symmetry of our system have been dropped (e.g.,  $A_j^0 \rightarrow A^0$ , etc.). Inserting the solution of the linear system  $\mathbf{D}(\rho, \mathbf{G})$  in expressions (32) yields  $A_j(\rho, \mathbf{G})$ .

In our reduced units the internal energy via the energy route (5) is given by

$$u = - \frac{2\pi\rho^2}{z_2} [x^2 G_{2;11} + \alpha x(1-x) G_{2;12} + \alpha x(1-x) G_{2;21} + (1-x)^2 G_{2;22}]. \quad (33)$$

The SCOZA closure relations (4) now read ( $i, j = 1, 2$ )

$$g_{ij}(r) = 0, \quad r < 1,$$

$$c_{ii}(r) = K_1(\rho) \frac{1}{r} e^{-z_1(\rho)(r-1)} + K_2(\rho, T, x) \frac{1}{r} e^{-z_2(\rho)(r-1)}, \quad r > 1,$$

$$c_{12}(r) = K_1(\rho) \frac{1}{r} e^{-z_1(\rho)(r-1)} + \alpha K_2(\rho, T, x) \frac{1}{r} e^{-z_2(\rho)(r-1)}, \quad r > 1. \quad (34)$$

The first terms on the right-hand side of the expression for the  $c_{ij}(r)$  in (34) represent the Waisman parametrization of the direct correlation function for the reference system:  $K_1(\rho)$  and  $z_1(\rho)$  are well-defined functions of  $\rho$  (see Appendix of Ref. 7).

The link between the MSA parameters  $\tilde{K}_{\nu;ij}$  and the SCOZA function  $K_2(\rho, T, x)$  is established via the following relations:

$$\tilde{K}_{1;ij} = K_1(\rho), \quad i, j = 1, 2,$$

$$\tilde{K}_{2;11} = \tilde{K}_{2;22} = K_2(\rho, T, x), \quad (35)$$

$$\tilde{K}_{2;12} = \tilde{K}_{2;21} = \alpha K_2(\rho, T, x).$$

We now go back to the SCOZA-PDE (11) and insert the  $A_j(\rho, \mathbf{G})$  of Eq. (30); this leads to

$$2 \sum_j x_j \frac{A_j}{(2\pi)^2} \sum_{\mu;rs} \frac{\partial A_j}{\partial G_{\mu;rs}} \frac{\partial G_{\mu;rs}}{\partial u} \frac{\partial u}{\partial \beta} = \rho \frac{\partial^2 u}{\partial \rho^2} \quad (36)$$

or

$$B(\rho, u) \frac{\partial u}{\partial \beta} = C(\rho) \frac{\partial^2 u}{\partial \rho^2} \quad (37)$$

with

$$B(\rho, u) = 2 \sum_j x_j \frac{A_j}{(2\pi)^2} \sum_{\mu;rs} \frac{\partial A_j}{\partial G_{\mu;rs}} \frac{\partial G_{\mu;rs}}{\partial u}, \quad (38)$$

$$C(\rho) = \rho.$$

We now have to determine  $A_j$ ,  $\partial A_j / \partial G_{\mu;rs}$ , and  $\partial G_{\mu;rs} / \partial u$  as functions of  $\rho$  and  $u$ . This is outlined in the following.

In a first step we determine  $\mathbf{G}$  for a given value of  $\rho$  and  $u$ : to this end we establish a set of eight nonlinear equations the solution of which gives  $\mathbf{G}(\rho, u)$ . The first of these relations is the energy equation (33) which is formally written as  $F_1(\rho, G_{2;11}, G_{2;12}, G_{2;21}, G_{2;22}, u) = 0$ . Further we consider Eq. (20) for  $\nu = 1$  and  $i, j = 1, 2$ : we have inserted the solution  $\mathbf{D}(\rho, \mathbf{G})$  of (21) and use (22) which has become  $A_{1;ij}^{(4)} = 2\pi K_1(\rho)$ ,  $i, j = 1, 2$ . We formally write these equations as  $F_i(\rho, \mathbf{G}) = 0$  ( $i = 2, \dots, 5$ ). The remaining three equations, written as  $F_i(\rho, \mathbf{G}) = 0$  ( $i = 6, \dots, 8$ ), are obtained from Eq. (20) for  $\nu = 2$  and eliminating the unknown function  $K_2(\rho, T, x)$  via the relations

$$A_{2;11}^{(4)} = A_{2;22}^{(4)}, \quad A_{2;12}^{(4)} = A_{2;21}^{(4)}, \quad A_{2;12}^{(4)} = \alpha A_{2;11}^{(4)}. \quad (39)$$

For given  $\rho$  and  $u$ , the  $\mathbf{G}$  are determined by solving the coupled set of eight nonlinear equations via a Newton–Raphson algorithm. Explicit expressions for the Jacobian,  $\mathcal{J}_{i,(\mu;rs)} = \partial F_i / \partial G_{\mu;rs}$  can be provided: for  $i = 1$ , these quantities are obtained from (33), while the remaining  $\mathcal{J}_{i,(\mu;rs)}$  are recovered from a differentiation of (20) with respect to the  $G_{\mu;rs}$ , e.g.,

$$\begin{aligned} \frac{\partial F_2}{\partial G_{\mu;rs}}(\rho, \mathbf{G}) = & \sum_l A_{\mu 1;sr1l}^{(1)} D_{\mu;sl} D_{1;1l} + \sum_{\tau,lmk} A_{\tau 1;mk1l}^{(1)} G_{\tau,km} \left( \frac{\partial D_{\tau,ml}}{\partial G_{\mu;rs}} D_{1;1l} + D_{\tau,ml} \frac{\partial D_{1;1l}}{\partial G_{\mu;rs}} \right) \\ & + \sum_{\tau} A_{\tau 1;m1l}^{(2)} \left( \frac{\partial D_{\tau,ml}}{\partial G_{\mu;rs}} D_{1;1l} + D_{\tau,ml} \frac{\partial D_{1;1l}}{\partial G_{\mu;rs}} \right) + A_{1;1l}^{(3)} \frac{\partial D_{1;1l}}{\partial G_{\mu;rs}} \end{aligned} \quad (40)$$

inserting  $\mathbf{D} = \mathbf{D}(\rho, \mathbf{G})$  and  $(\partial \mathbf{D} / \partial \mathbf{G})(\rho, \mathbf{G})$  from solutions of the linear equations (23) and (29). Similar expressions can be derived for the other derivatives.

The  $\mathbf{G}(\rho, u(\rho, \beta - \Delta\beta))$  from the previous temperature step in the solution algorithm of the PDE (37) are taken as initial values of the Newton–Raphson technique. In each step of the iteration, for given  $\mathbf{G}$  the linear system (23) is solved yielding  $\mathbf{D}(\rho, \mathbf{G})$ . Then the derivatives  $(\partial D_{\tau,ml} / \partial G_{\mu;rs})(\rho, \mathbf{G})$  are obtained by solving the linear equations (29). These solutions are inserted in the expression for  $\mathcal{J}$ . Convergence in the Newton–Raphson method is achieved if the relative difference of two successive values of  $\mathbf{G}$  is less than  $10^{-10}$ . Furthermore it is checked whether the solution is physical, i.e., if  $G_{2;12} = G_{2;21}$ . With this solution  $\mathbf{G}(\rho, u)$  one calculates  $\mathbf{D}(\rho, u) = \mathbf{D}(\rho, \mathbf{G}(\rho, u))$  via (23),  $A_j(\rho, u)$  via (31) and (32), and  $(\partial \mathbf{D} / \partial \mathbf{G})(\rho, u)$  via (29).

We now proceed to calculate the coefficient functions of the SCOZA–PDE (37). The derivatives  $(\partial A_j / \partial G_{\mu;rs})(\rho, u)$  required in (38) are obtained from (31) and are given by

$$\frac{\partial A_j}{\partial G_{\mu;rs}} = A^0 \frac{\partial M_j}{\partial G_{\mu;rs}} - 4B^0 \frac{\partial N_j}{\partial G_{\mu;rs}}, \quad (41)$$

where

$$\begin{aligned} \frac{\partial M_j}{\partial G_{\mu;rs}} = & - \sum_{\tau} \frac{1}{z_{\tau}^2} \sum_m \rho_m \left\{ M_{\tau}^{(a)} \frac{\partial D_{\tau,mj}}{\partial G_{\mu;rs}} \right. \\ & \left. + (1 - M_{\tau}^{(a)} e^{-z_{\tau}}) \frac{\partial f_{\tau,mj}}{\partial G_{\mu;rs}} \right\}, \\ \frac{\partial N_j}{\partial G_{\mu;rs}} = & \sum_{\tau} \frac{1}{z_{\tau}^3} \sum_m \rho_m \left\{ L_{\tau}^{(a)} \frac{\partial D_{\tau,mj}}{\partial G_{\mu;rs}} \right. \\ & \left. + (1 - L_{\tau}^{(a)} e^{-z_{\tau}}) \frac{\partial f_{\tau,mj}}{\partial G_{\mu;rs}} \right\}, \quad (42) \\ \frac{\partial f_{\tau,mj}}{\partial G_{\mu;rs}} = & \frac{2\pi}{z_{\tau}^2} \sum_k \rho_k \left( \delta_{\mu\tau} \delta_{mr} \delta_{ks} D_{\tau,kj} \right. \\ & \left. + G_{\tau,mk} \frac{\partial D_{\tau,kj}}{\partial G_{\mu;rs}} \right). \end{aligned}$$

The derivatives  $\partial G_{\mu;rs} / \partial u$  are obtained by implicitly differentiating the equations  $F_i = 0$  ( $i = 1, \dots, 8$ ) with respect to  $u$ ; inversion by use of the Jacobian  $\mathcal{J}$  leads to

$$\begin{pmatrix} \frac{\partial G_{1;11}}{\partial u} \\ \frac{\partial G_{1;12}}{\partial u} \\ \vdots \\ \frac{\partial G_{2;22}}{\partial u} \end{pmatrix} = \mathcal{J}^{-1} \cdot \begin{pmatrix} -1 \\ 0 \\ \vdots \\ 0 \end{pmatrix}. \quad (43)$$

Inserting the values of  $\mathbf{G}(\rho, u)$ ,  $\mathbf{D}(\rho, \mathbf{G}(\rho, u))$ , and  $(\partial \mathbf{D} / \partial \mathbf{G})(\rho, u)$  in Eqs. (41) and (42) in  $\mathcal{J}$  of (43) finally gives  $(\partial A_j / \partial G_{\mu;rs})(\rho, u)$  and  $(\partial \mathbf{G} / \partial u)(\rho, u)$ . Now, the SCOZA–PDE (37) is ready for being solved. Numerical details for its solution are presented in Sec. II D.

Once  $u(\rho, T, x)$  has been determined the quantities relevant for the calculation of the phase diagram, the pressure  $P$  and the chemical potentials  $\mu_i$  ( $i = 1, 2$ ), are obtained by integrating  $\partial \beta P / \partial \beta$  and  $\partial \beta \mu_i / \partial \beta$  with respect to  $\beta$  via

$$\frac{\partial \beta \mu_1}{\partial \beta} = \frac{\partial u}{\partial \rho} + \frac{1-x}{\rho} \frac{\partial u}{\partial x}, \quad (44)$$

$$\frac{\partial \beta \mu_2}{\partial \beta} = \frac{\partial u}{\partial \rho} - \frac{x}{\rho} \frac{\partial u}{\partial x}, \quad (45)$$

$$\frac{\partial \beta P}{\partial \beta} = -u + \rho \frac{\partial u}{\partial \rho}, \quad (46)$$

with the Carnahan–Starling values<sup>26</sup> for  $\beta P$  and  $\beta \mu_i$  as integration constants at  $\beta = 0$

$$\beta P(\rho, \beta = 0, x) = \rho \frac{1 + \eta + \eta^2 - \eta^3}{(1 - \eta)^3}, \quad (47)$$

$$\beta \mu_i(\rho, \beta = 0, x) = \ln \rho_i + \frac{8\eta - 9\eta^2 - 3\eta^3}{(1 - \eta)^3}. \quad (48)$$

$\eta = (\pi/6)\rho$  is the packing fraction. The symmetry of the system induces symmetry relations in the correlation functions and hence in the thermodynamic properties. For instance, for the chemical potentials and for the pressure we find

$$\mu_1(\rho, T, x) = \mu_2(\rho, T, 1 - x), \quad (49)$$

$$P(\rho, T, x) = P(\rho, T, 1 - x). \quad (50)$$

#### D. Numerical solution

As a consequence of the simplifying assumption (10) the SCOZA–PDE is now only a PDE in  $\beta$  and  $\rho$ , which can be

solved for different  $x$  values independently. The SCOZA–PDE (37) is a nonlinear diffusion equation, that has been solved by an implicit finite-difference algorithm<sup>27</sup> described in detail in Ref. 28 on a  $(\beta, \rho)$ -grid  $[0, \beta_f] \times [0, \rho_0]$ ; the grid-size in  $\rho$ ,  $\Delta\rho$ , is 0.001,  $\Delta\beta$  is in general  $10^{-5}$ , but becomes even smaller in the liquid–vapor critical region, and  $\Delta x = 0.01$  with  $x \in [0, 1/2]$ . In contrast to conventional liquid state theories the SCOZA can be solved even in the critical regions.

Integration with respect to  $\beta$  starts at  $\beta=0$  and then proceeds to lower temperatures. At each temperature the nonlinear equations  $F_i=0$  (introduced in the preceding section) are solved, leading to the  $\mathbf{G}(\rho, u)$ : to ensure rapid convergence the values of the  $\mathbf{G}(\rho, u)$  obtained at the previous temperature step ( $\beta - \Delta\beta$ ) in the solution algorithm of the PDE are taken as initial guess for the solution of the system of nonlinear equations at  $\beta$ . In the next step,  $\mathbf{D}(\rho, u)$ ,  $A_j(\rho, u)$ ,  $\partial\mathbf{D}/\partial\mathbf{G}$ ,  $\partial A_j/\partial\mathbf{G}$ , and  $\partial\mathbf{G}/\partial u$  are calculated, from which we calculate the coefficient function  $B(\rho, u)$  via (38).

For the boundary condition we have used for  $\rho=0$

$$u(\rho=0, \beta, x) = 0 \quad \text{for all } \beta \text{ and all } x \quad (51)$$

and for the boundary condition at high density ( $\rho_0=1$ ) we make use of the high temperature approximation (HTA):<sup>2</sup> this approximation is known to be very accurate for high densities such that for a sufficiently large value of  $\rho_0$  a boundary condition based on the HTA should be reasonably good.

For the initial condition at  $\beta=0$  we assume that the direct correlation functions coincide with those of a HC system. Explicit expressions for these functions are obtained from the MSA formalism, by setting  $\tilde{K}_{\nu;ij}=0$  for all  $i$  and  $j$  and for  $\nu=2$ . For details we refer to Ref. 8.

## E. Thermodynamic stability

To find out the limits of thermodynamic stability becomes for a fluid mixture a considerably more complex problem than in the one component case: now, for a given composition, density, and temperature the requirements for both mechanical *and* material stability must be fulfilled. Mechanical stability is expressed (similar as in the one component case) via  $\chi_T > 0$ , while material stability is expressed via the criterion

$$\left( \frac{\partial^2 G}{\partial x^2} \right)_{T, P, \rho} \geq 0, \quad (52)$$

where  $G$  is the Gibbs free energy of the system.

It is more convenient to trace back the above two stability criteria to the long-wavelength limit of two structure factors, the number–number  $S_{NN}(q)$  and the concentration–concentration  $S_{cc}(q)$  structure factors which are suitable linear combinations of the Fourier transforms of the direct correlation functions,  $h_{ij}(r)$ :

$$\begin{aligned} S_{NN}(q) &= 1 + \rho \{ x^2 \tilde{h}_{11}(q) + (1-x)^2 \tilde{h}_{22}(q) \\ &\quad + 2x(1-x) \tilde{h}_{12}(q) \}, \\ S_{cc}(q) &= x(1-x) \{ 1 + \rho x(1-x) [ \tilde{h}_{11}(q) + \tilde{h}_{22}(q) \\ &\quad - 2 \tilde{h}_{12}(q) ] \}, \\ S_{Nc}(q) &= \rho x(1-x) \{ x [ \tilde{h}_{11}(q) - \tilde{h}_{12}(q) ] \\ &\quad - (1-x) [ \tilde{h}_{22}(q) - \tilde{h}_{12}(q) ] \}. \end{aligned} \quad (53)$$

Their long-wavelength limits are related to the thermodynamic properties via<sup>29</sup>

$$\begin{aligned} S_{NN}(0) &= \chi_T + \delta^2 S_{cc}(0), \\ S_{cc}(0) &= \frac{Nk_B T}{\left( \frac{\partial^2 G}{\partial x^2} \right)_{T, P, \rho}}, \\ S_{Nc}(0) &= -\delta S_{cc}(0) \end{aligned} \quad (54)$$

with  $\delta = \rho(\bar{v}_1 - \bar{v}_2)$  where the  $\bar{v}_i$  are the partial molar volumes.

From the above criteria for stability it follows that as we reach the limits of mechanical stability,  $S_{NN}(0)$  diverges, while at the border of material stability  $S_{cc}(0)$  diverges. In addition, one also considers the (sub-)case of the so-called azeotropic instability, where the mixture is mechanically unstable (i.e., diverging compressibility) while remaining materially stable [i.e., finite  $S_{cc}(0)$ ]. The spinodal of a mixture is thus located at those points where either  $S_{NN}(0)$  or  $S_{cc}(0)$  or both diverge.

Arrieta *et al.*<sup>12</sup> have shown that if any of the above instabilities occurs, then the quantity  $\Delta(0)$ , defined as

$$\begin{aligned} \Delta(0) &= \{ \det [ \delta_{ij} + \sqrt{\rho_i \rho_j} \tilde{h}_{ij}(0) ] \}^{-1/2} \\ &= \{ \det [ \delta_{ij} - \sqrt{\rho_i \rho_j} \tilde{c}_{ij}(0) ] \}^{1/2} \\ &= \det ( \delta_{ij} - \sqrt{\rho_i \rho_j} \bar{Q}_{ij} ) \end{aligned} \quad (55)$$

becomes zero. As also outlined in Ref. 12,  $\Delta(0)$  can readily be calculated from parameters available from the MSA solution:

$$\begin{aligned} \bar{Q}_{ij} &= \int_0^\infty Q_{ij}(r) dr \\ &= \frac{1}{6} A_j - \frac{1}{2} b_j - \sum_\tau \frac{1}{z_\tau^2} (C_{\tau;ij} M_\tau^{(a)} - f_{\tau;ij}) \end{aligned} \quad (56)$$

with

$$b_j = b_0(1 + M_j) + A^0 N_j, \quad (57)$$

$$C_{\tau;ij} = f_{\tau;ij} e^{-z_\tau r} - D_{\tau;ij}, \quad (58)$$

and Eqs. (31) and (32).  $b_0$  is calculated from  $\rho$  and  $\sigma$  (see Appendix A of Ref. 12).

Of course from  $\Delta(0)=0$  we do not learn which limit of instability is actually reached; this has to be decided in a more detailed investigation. It should also be noted, that the

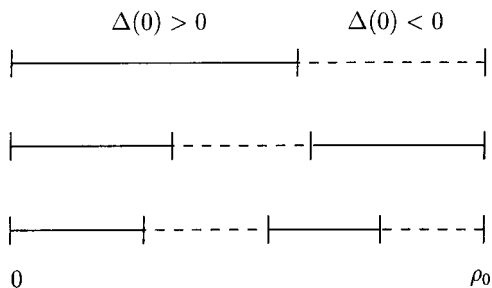


FIG. 1. The three different cases of the instability region on the interval  $[0, \rho_0]$  for a given value of  $x$  and  $T$  for a HCY fluid. The full lines are the stable regions where  $\Delta(0) > 0$ , while the dashed lines represent the unstable regions that are excluded from the integration of the SCOZA-PDE.

sign of  $\Delta(0)$  plays an important role when deciding whether an MSA solution is acceptable for a given system: Pastore has shown rigorously<sup>25</sup> that if  $\Delta(0) \leq 0$  then the solution has to be rejected. On the other hand, the fact that  $\Delta(0)$  is positive does not guarantee that the solution is physical: only the fact that  $\Delta(s)$  has no zero in the complex right half-plane of  $s$  is a criterion that the solution is physical (and hence unique<sup>25</sup>). However, it has turned out,<sup>12</sup> that the simpler criterion, i.e.,  $\Delta(0) > 0$ , is very reliable to detect physical solutions.

We have used the “ $\Delta(0) > 0$ ” criterion in our calculations to determine the spinodal and assume—according to the simplified criterion outlined above—that it also separates physical (and hence unique) solutions from unphysical solutions of the MSA/SCOZA. From the numerical point of view we proceeded as follows: the boundary conditions on the spinodal lines are

$$u(\rho_S, \beta) = u_S(\rho_S), \tag{59}$$

where the density  $\rho_S$  is the approximation for the spinodal density on the discrete density grid at a given temperature. It is located at that grid-point where  $\Delta(0)$  changes sign and

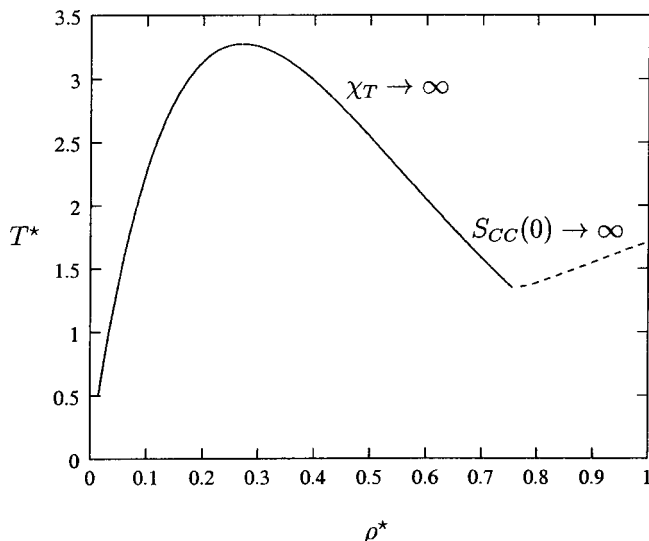


FIG. 2. Spinodal line in the  $(\rho^*, T^*, x=1/2)$  plane for an equimolar binary HCY mixture with  $\alpha=0.9$  and  $z\sigma=0.8$ . Different line symbols are used for the density regimes in which either  $\chi_{red}$  (full line) or  $S_{cc}(0)$  (dashed line) diverge.

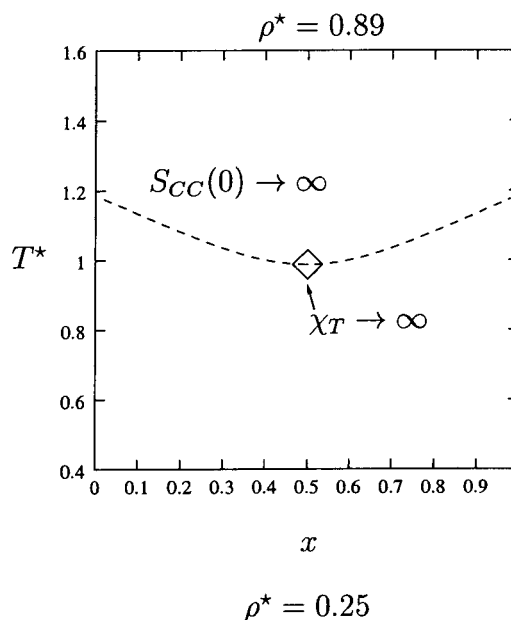
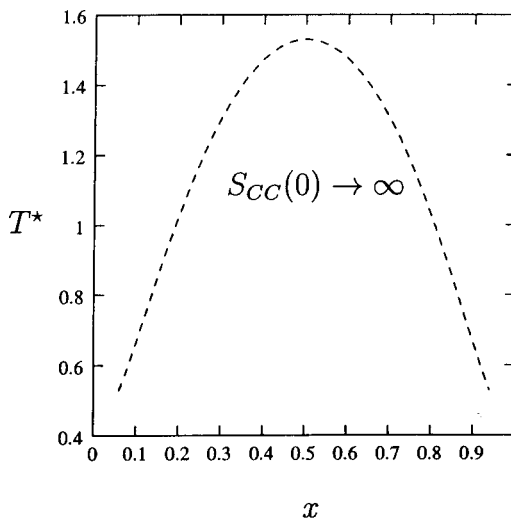


FIG. 3. Phase stability lines in the  $(T^*, x)$  plane for a HCY mixture with  $\alpha=0.65$  and  $z\sigma=1.8$ . The point where  $\chi_{red}$  diverges is marked by a diamond. Everywhere else  $S_{cc}(0)$  diverges (dashed line).

becomes negative.  $u_S(\rho)$  is the value of the excess internal energy where  $\Delta(0)=0$ . This value is determined from the set of eight nonlinear equations

$$\begin{aligned} \Delta(0)(\rho, \mathbf{G}) &= 0, \\ F_i(\rho, \mathbf{G}) &= 0, \quad i = 2, \dots, 8, \end{aligned} \tag{60}$$

with the functions  $F_i$  introduced above. These equations are solved for  $\mathbf{G}$  using a Newton-Raphson technique where the Jacobian of the nonlinear system is provided. This Jacobian can be calculated in a straightforward way analogous to the one in Sec. II C. Inserting the solution  $\mathbf{G}(\rho)$  in the energy equation (33) finally yields  $u_S(\rho)$ . For the binary symmetric HCY fluid that we have investigated, three cases of instability regions in the interval  $[0, \rho_0]$  for a given value of  $x$  and  $T$  have to be distinguished that are shown in Fig. 1.

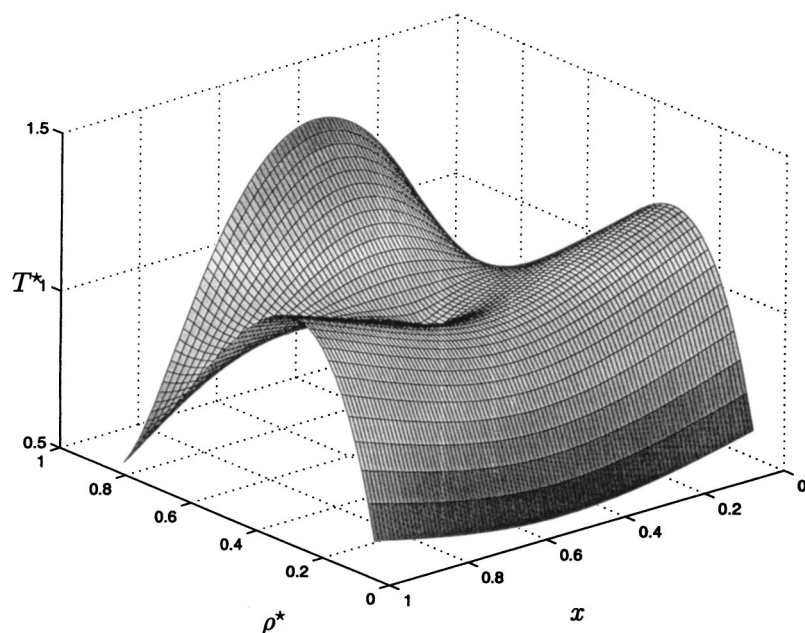


FIG. 4. Three-dimensional view of the spinodal curve of a symmetric binary HCY mixture with  $\alpha=0.65$  and  $z\sigma=1.8$  in the  $(\rho^*, T^*, x)$  space.

### III. RESULTS

We present results for the stability and for the phase diagram of a binary symmetric mixture determined via the SCOZA. Now that the number of system parameters is reduced substantially the phase behavior of such a system can be studied very easily in a systematic way; as noted above the unique parameter that triggers the phase behavior is  $\alpha$ , the ratio between the unlike and the like interaction. A mean-field study by Wilding *et al.*<sup>3</sup> has already revealed the phase behavior of such a system in a qualitative way. We expect four phases which we denote as follows: the vapor (G), the mixed fluid (MF) and two phases of a demixed fluid (DF)—a 1-rich and a 2-rich fluid; the latter ones are often counted—as a consequence of the symmetry with respect to  $x$ —as one single phase. For convenience we introduce the reduced dimensionless density  $\rho^* = \rho\sigma^3 = \rho$  and the reduced dimensionless temperature  $T^* = k_B T \sigma / K_{11} = k_B T$ .

#### A. Thermodynamic stability

We start our discussion on the stability of our system with a projection of the three-dimensional spinodal onto the  $(\rho^*, T^*, x=1/2)$ -plane, shown in Fig. 2. The stable phases lie (as also in the following plots) above the spinodal line. The curve shown in Fig. 2 consists of two parts that intersect at a threshold density  $\rho_t^* \sim 0.76$ : for  $\rho^* < \rho_t^*$ ,  $\chi_{\text{red}}$  diverges while  $S_{cc}(0)$  remains finite, while for  $\rho^* > \rho_t^*$ ,  $S_{cc}(0)$  diverges while the compressibility remains finite.  $\rho_t^*$  is  $\alpha$  dependent; this has been discussed in detail in Ref. 30.

We then proceed to a projection of the spinodal onto the  $(T^*, x)$  plane, shown in Fig. 3 for two different  $\rho^*$  values, one of them being below, the other one being above  $\rho_t^*$  of this system. For the higher density, all points of the spinodal are characterized by a divergence of  $S_{cc}(0)$ , while for the density smaller than  $\rho_t^*$ ,  $S_{cc}(0)$  diverges everywhere except for  $x=1/2$  where  $\chi_{\text{red}}$  diverges. We also observe that the curvature of the projections of the spinodal on the  $(T^*, x)$  plane changes as the density is varied. Physical reasons for this

observation are, for instance, discussed in Ref. 31.

A three-dimensional plot of the spinodal in the  $(\rho^*, T^*, x)$  space is shown in Fig. 4. Let us approach this stability boundary from above on different paths: we fix the concentration  $x$  to  $1/2$ , choose some density and reduce the temperature until we reach the stability boundary. If we reduce, for a given density larger than the threshold value ( $\rho^* > \rho_t^*$ ), the temperature until we cross the stability boundary where  $S_{cc}(0)$  diverges, self-aggregation will take place and the fluid will demix into a 1-rich and a 2-rich phase (DF). For  $\rho^* < \rho_t^*$ , where  $\chi_{\text{red}} \rightarrow \infty$  the fluid becomes mechanically unstable and separates into a MF and a G phase. Finally, by further reducing the density the scenario will again change and the fluid will decompose into three phases: a G phase and two DF phases.

#### B. Phase diagrams

The phase diagram is calculated by solving the coexistence equations, i.e. equal chemical potentials and equal pressure of the coexisting phases at a given temperature. We characterize coexisting phases by  $(\rho, x)$  and  $(\rho', x')$  and proceed as follows: the G–MF coexistence curve is obtained by solving the set of equations

$$\mu_i(\rho, T, x=1/2) \equiv \mu(\rho, T, x=1/2) = \mu(\rho', T, x=1/2), \quad (61)$$

$$P(\rho, T, x=1/2) = P(\rho', T, x=1/2). \quad (62)$$

For the G–MF and the MF–DF transitions we proceed in two steps: first we determine the phase diagram of the demixing transition, i.e., looking at a given temperature  $T$  for two coexisting states with the same fluid density but different composition by fixing  $\rho = \rho'$  and by determining concentrations  $x$  and  $x' = 1 - x$  of the coexisting phases. The equilibrium condition for the pressure is automatically fulfilled, while the equilibrium conditions for the chemical potentials become at given  $T$  and  $\rho$

$$\mu_1(\rho, T, x) = \mu_2(\rho, T, x) \quad (63)$$

which defines (if it exists) the line  $x(\rho)$  of the second order demixing transition. Along this line the chemical potentials of the two species are equal by construction; they are denoted by  $\mu[T, \rho, x(\rho)]$ . In a second step the solution of the two equations

$$\mu[\rho, T, x=1/2] = \mu[\rho', T, x(\rho')], \quad (64)$$

$$P[\rho, T, x=1/2] = P[\rho', T, x(\rho')] \quad (65)$$

gives the density  $\rho$  of the G or MF and the density  $\rho'$  of the DF with concentrations  $x(\rho')$  and  $1-x(\rho')$ , in equilibrium.

We only consider the more interesting case where  $\alpha < 1$ : here we observe a competition between the G–MF transition and the demixing transition. According to the loci where the  $\lambda$  line (i.e., the critical line of the demixing transitions) intersects the second order G–MF transition one can distinguish three types of phase diagrams. In Figs. 5 and 6 we show the  $(\rho^*, T^*)$  phase diagrams of two binary symmetric mixtures for three different values of  $\alpha$  (as indicated); they are projections of the three-dimensional  $(\rho^*, T^*, x)$  diagrams onto the  $(\rho^*, T^*)$  plane. The  $\alpha$  values are chosen so that each of the types of phase diagrams is represented. (i) In the type I case, the  $\lambda$  line approaches the G–MF coexistence curve well below the critical point; the intersection point is called a CEP: here, a critical liquid coexists with a noncritical gas. Above  $T_{\text{CEP}}$  a gas and a homogeneous liquid of intermediate density coexist, becoming identical at the G–MF critical point. When increasing  $\rho$ , the liquid demixes as one crosses the  $\lambda$  line. The (full) curve below the CEP temperature (cf. bottom panels in Figs. 5 and 6) is a triple line where a gas, a 1-rich and a 2-rich liquid coexist. (ii) In the type III case the  $\lambda$  line intersects the G–MF curve at the G–MF critical point. Now there is no first order transition between the gas and the mixed liquid and the  $\lambda$  line ends at a tricritical point where three phases become critical at the same time: a gas, a 1-rich and a 2-rich liquid. Two order parameters, the difference in the coexisting liquid and vapor densities, and the concentration difference vanish at the same time. (iii) Finally, type II represents the intermediate case, where the  $\lambda$ -line intersects the G–MF coexistence curve slightly below the critical point. One finds—as in type I—a critical point of the G–MF transition and, similar as in type III, a tricritical point. In addition, we observe a triple point where a gas, a mixed liquid at intermediate density, and a 1-rich and a 2-rich liquid at high density coexist.

Concluding, it should be pointed out that similar archetypes of phase diagrams are also encountered in other liquid systems with completely different interatomic interactions, such as the Heisenberg fluid<sup>32</sup> or the Stockmayer fluid.<sup>33</sup>

#### IV. CONCLUSION

The SCOZA is an advanced liquid state method that is known to give reliable results for continuous one component systems even in the critical region. This is achieved by enforcing thermodynamic self-consistency between the compressibility and the energy route via a state dependent function  $K(\rho, T)$  which is determined by solving a PDE. In this

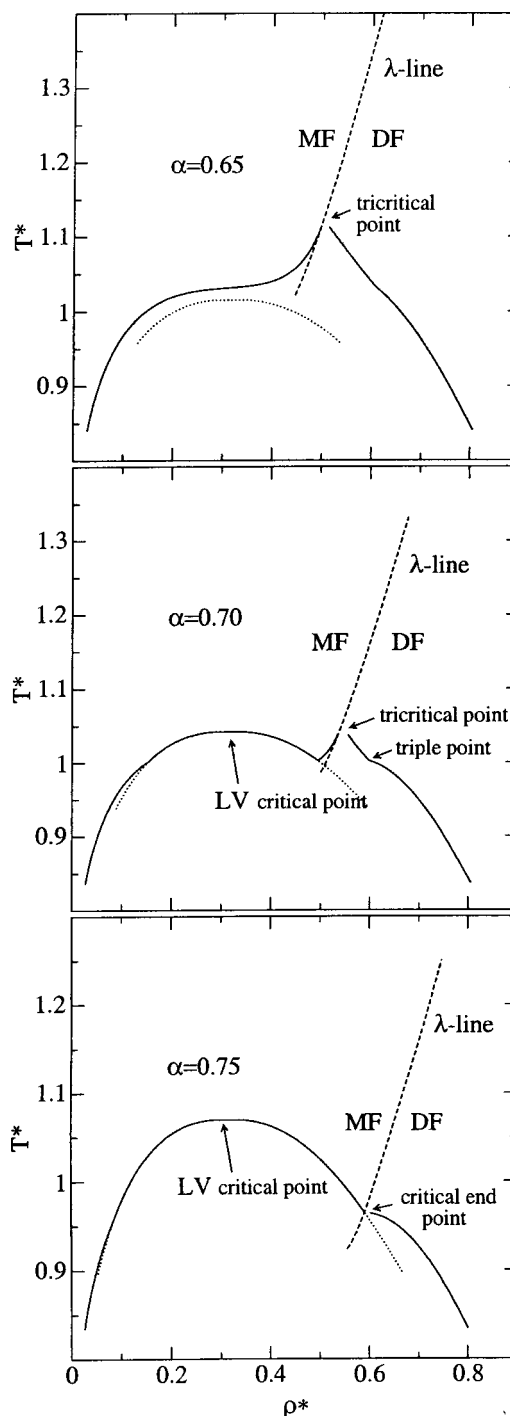


FIG. 5. SCOZA phase diagrams in the  $(\rho^*, T^*)$  plane for various  $\alpha$  values and  $z\sigma=1.8$ . The full lines represent first-order phase coexistence, the dashed lines the  $\lambda$  line and the dotted curves metastable G–MF transitions.

contribution we have generalized the formalism of the SCOZA to the case of a binary symmetric mixture. Introducing an approximation on the now three yet undetermined, state-dependent functions  $K_{ij}(\rho, \beta, x)$  we can reduce the three coupled PDEs (for  $u$  in  $\rho$ ,  $T$ , and  $x$ ) to one single PDE for  $u$  in  $T$  and  $\rho$ . In the first part of this paper we have presented the formalism, we have given details of the numerical solution of the PDE and have discussed stability criteria of binary mixtures. Assuming a simple HCY interaction for the interatomic potentials we have then calculated the

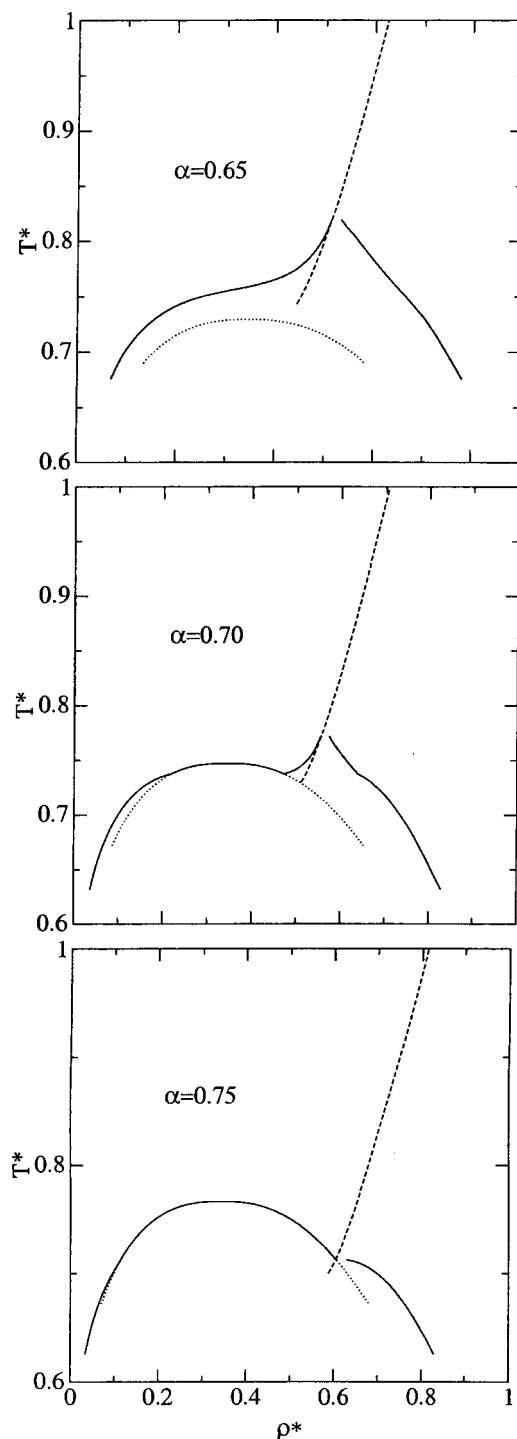


FIG. 6. The same as in Fig. 5 for  $z\sigma=2.5$ .

phase diagram of such a system. Varying the parameter  $\alpha$ , i.e., the ratio between the like and the unlike interactions, we encounter three archetypes of phase diagrams characterized by the intersection of the line of the second order demixing transition and the first order liquid–vapor coexistence curve, each of them characterized by a specific critical behavior. In contrast to conventional liquid state theories, the coexistence curves can be determined also very close to the critical point, offering thus the possibility to study critical phenomena on a quantitative level.

## ACKNOWLEDGMENTS

This work was supported by the Österreichische Forschungsfond under Project Nos. P13062-TPH and P15758-TPH. E.S.P. was supported by the Graduate Program “Computational Material Science” of the Österreichische Forschungsfond (Project No. W004). Both authors are indebted to Professor D. Levesque and Professor J.-J. Weis for many stimulating discussions and are grateful for the warm hospitality at the Laboratoire de Physique Théorique (Université Paris Sud, Orsay), where part of this work was done. Many stimulating and helpful discussions with Professor G. Stell (Stony Brook) are gratefully acknowledged.

- <sup>1</sup>P. H. van Konynenburg and R. L. Scott, *Philos. Trans. R. Soc. London, Ser. A* **51**, 495 (1980).
- <sup>2</sup>J.-P. Hansen and I.R. McDonald, *Theory of Simple Liquids*, 2nd ed. (Academic, New York, 1986).
- <sup>3</sup>N. B. Wilding, F. Schmid, and P. Nielaba, *Phys. Rev. E* **58**, 2201 (1998).
- <sup>4</sup>D. Levesque and J.-J. Weis (unpublished).
- <sup>5</sup>R. Dickman and G. Stell, *Phys. Rev. Lett.* **77**, 996 (1996).
- <sup>6</sup>A. Parola and L. Reatto, *Adv. Phys.* **44**, 211 (1995).
- <sup>7</sup>D. Pini, G. Stell, and N. B. Wilding, *Mol. Phys.* **95**, 483 (1998); *J. Chem. Phys.* **115**, 2702 (2001).
- <sup>8</sup>G. Kahl, E. Schöll-Paschinger, and G. Stell, *J. Phys.: Condens. Matter* **14**, 9153 (2002); E. Schöll-Paschinger, Ph.D. thesis, Technische Universität Wien, 2002; thesis available from the homepage <http://tph.tuwien.ac.at/~paschinger/> and download “PhD.”
- <sup>9</sup>A. Reiner and G. Kahl, *Phys. Rev. E* **65**, 051 104 (2002); A. Reiner, Ph.D. thesis, Technische Universität Wien, 2002; thesis available at <http://purl.oclc.org/NET/a-reiner/dr-thesis/>
- <sup>10</sup>L. S. Ornstein and F. Zernike, *Proc. R. Acad. Sci. Amsterdam* **17**, 1452 (1914).
- <sup>11</sup>A. G. Dickman and G. Stell, *Mol. Phys.* **100**, 3021 (2002).
- <sup>12</sup>E. Arrieta, C. Jędrzejek, and K. N. Marsh, *J. Chem. Phys.* **95**, 6806 (1991).
- <sup>13</sup>D. Pini, A. Parola, and L. Reatto, *J. Stat. Phys.* **100**, 13 (2000).
- <sup>14</sup>D. Pini, M. Tau, A. Parola, and L. Reatto, *Phys. Rev.* (to be published).
- <sup>15</sup>E. Waisman, *Mol. Phys.* **25**, 45 (1973).
- <sup>16</sup>E. Schöll-Paschinger, D. Levesque, J.-J. Weis, and G. Kahl (unpublished).
- <sup>17</sup>E. Waisman, J. S. Høye, and G. Stell, *Chem. Phys. Lett.* **40**, 514 (1976); J. S. Høye, G. Stell, and E. Waisman, *Mol. Phys.* **32**, 209 (1976); J. S. Høye and G. Stell, *ibid.* **52**, 1057 (1984).
- <sup>18</sup>J. S. Høye and G. Stell, *Mol. Phys.* **52**, 1071 (1984).
- <sup>19</sup>M. Wertheim, in *The Equilibrium Theory of Classical Fluids*, edited by H. Frisch and J. Lebowitz (Benjamin, New York, 1964), p. II-268.
- <sup>20</sup>R. J. Baxter, *Aust. J. Phys.* **21**, 563 (1968).
- <sup>21</sup>L. Blum and J. S. Høye, *J. Stat. Phys.* **19**, 317 (1978).
- <sup>22</sup>L. Blum, *J. Stat. Phys.* **22**, 661 (1980).
- <sup>23</sup>L. Blum, F. Vericat, and J. N. Herrera-Pacheco, *J. Stat. Phys.* **66**, 249 (1992).
- <sup>24</sup>L. Blum and J. N. Herrera, *Mol. Phys.* **95**, 425 (1998).
- <sup>25</sup>G. Pastore, *Mol. Phys.* **55**, 187 (1988).
- <sup>26</sup>N. F. Carnahan and K. E. Starling, *J. Chem. Phys.* **51**, 635 (1969).
- <sup>27</sup>F. W. Ames, *Numerical Methods for Partial Differential Equations* (Academic, New York, 1977).
- <sup>28</sup>D. Pini, G. Stell, and R. Dickman, *Phys. Rev. E* **57**, 2862 (1998).
- <sup>29</sup>A. B. Bhatia and D. E. Thornton, *Phys. Rev. B* **2**, 3004 (1970).
- <sup>30</sup>C. Caccamo, G. Giunta, and C. Hoheisel, *Phys. Lett. A* **158**, 325 (1991).
- <sup>31</sup>C. Caccamo and G. Giunta, *Mol. Phys.* **78**, 83 (1993).
- <sup>32</sup>J.-J. Weis, M. J. P. Nijmeijer, J. M. Tavares, and M. M. Telo da Gama, *Phys. Rev. E* **55**, 436 (1997); J. M. Tavares, M. M. Telo da Gama, P. I. C. Teixeira, J.-J. Weis, and M. J. P. Nijmeijer, *ibid.* **52**, 1915 (1995).
- <sup>33</sup>B. Groh and S. Dietrich, *Phys. Rev. Lett.* **72**, 2422 (1994); in *New Approaches to Problems in Liquid State Theory*, edited by C. Caccamo, J.-P. Hansen, and G. Stell, *Nato Science Series* (Kluwer, Dordrecht, 1999).